Error Estimation Procedure for Plate Bending Elements

John O. Dow* and Doyle E. Byrd†
University of Colorado, Boulder, Colorado

Procedures for identifying and eliminating errors inherent in individual finite elements and those due to the discretization of the continuum are presented. The elemental errors are identified through the use of an element formulation procedure based on physically interpretable strain-gradient interpolation functions. The use of this notation allows these errors to be eliminated using rational arguments. The discretization errors are identified by comparing the finite-element solution to a smoothed superconvergent solution. The errors thus identified are used to guide an adaptive mesh refinement procedure that produces improved results.

I. Introduction

THE finite-element method represents the continuum by subdividing it into a number of small regions. This approximate representation introduces two distinct types of error. The first source of error is the modeling deficiencies contained in the elements themselves. The second source of error results from the discretization of the continuum. This paper presents a simple and accurate error estimation procedure for plate-bending problems that computes the combined effects of both types of error.

The artificial stiffening errors associated with the modeling deficiencies in the elements have conventionally been labeled as either "shear locking" or "parasitic shear," without distinction between the two phenomena. In this paper the two phrases will be used to describe two distinct phenomena. The error due to parasitic shear will be shown to be caused by the use of incomplete polynomials in the generation of the element. It is this error that is usually referred to by the two mentioned phrases. The use of "reduced integration" in the generation of elements is an attempt to eliminate the effects of parasitic shear. The other phenomenon, termed in this paper as shear locking, is not as widely known but has received attention in recent years. Shear locking occurs independently of parasitic shear and is an error in the mathematical modeling of the physical system. This misrepresentation allows the shear strain energy to become unbounded in the mathematical model, whereas in the physical system this is impossible. This modeling deficiency is illustrated in this paper with ways of controlling the growth of the shear strain given.

Both local and global discretization error estimates are computed. The global errors are found by summing the estimated errors for the individual elements. The local error estimates are used to guide model refinements that result in more accurate solutions. This procedure will be illustrated in a later section.

The discretization errors are estimated in a two-step process. A smoothed superconvergent solution is first computed from the finite-element result. Then the error measures are computed by comparing the energy norms of the smoothed solution to those contained in the unmodified finite-element solution.

The element modeling errors described affect the discretization errors in the overall solution. The effect of these errors is shown by comparing the error levels found in identical problems modeled with corrected and uncorrected elements. The modeling deficiencies contained in the individual elements are identified through the use of strain-gradient-based interpolation functions. The use of this physically interpretable notation allows the modeling characteristics of the finite element to be related directly to the physical quantities being modeled. It is this direct relation between the mathematical model and the physical system that allows the source of the modeling deficiencies to be identified. With the errors rationally defined, it is a straightforward operation to eliminate them. This notation and the error estimation procedure are presented in the next section.

II. Theoretical Background

A. Strain-Gradient-Based Finite Elements

The use of strain-gradient notation in the derivation of finite-element stiffness matrices has been developed by the authors with detailed presentations given elsewhere.[1-5] The basic premise behind the use of the strain-gradient notation is that the usual unknown coefficients, sometimes known as generalized coordinates, in the displacement polynomials can be defined in terms of physically interpretable strain-gradient coefficients. This is similar to a Taylor series expansion of the displacements in terms of the displacements and their derivatives. A brief presentation of the strain-gradient approach to the derivation of Mindlin plate-bending elements is included in a later section. An example of this notation is given the following polynomial representation for the out-of-plane displacement of a four-node Mindlin plate element:

$$w = w_{rb} + (\gamma_{xz}/2 - q_{rb})x + (\gamma_{yz}/2 + p_{rb})y + \left((-\gamma_{xy,z} + \gamma_{yz,x} + \gamma_{xz,y})/2\right)xy \tag{1}$$

$$w = [1 \quad y \quad -x \quad x/2 \quad -xy/2 \quad xy/2 \quad xy/2]\{\epsilon\}$$

where

$$\{\epsilon\} = [w_{rb} \quad p_{rb} \quad q_{rb} \quad \gamma_{xz} \quad \gamma_{yz} \quad \gamma_{xy,z} \quad \gamma_{yz,x} \quad \gamma_{xz,y}]^T$$

The subscript *rb* denotes rigid-body modes of deformation. A term like $\gamma_{xy,z}$ is the derivative with respect to z of the shear strain γ_{xy}.

Received March 25, 1988; presented as Paper 88-1415 at the AIAA/ASME/ASCE/AHS 29th Structures, Structural Dynamics and Materials Conference, Williamsburg, VA, April 18-20, 1988; revision received Jan. 30, 1989.

*Associate Professor, Department of Civil, Environmental, and Architectural Engineering; currently on leave at University College of Swansea, Civil Engineering Department.

†Graduate Research Assistant, Department of Civil, Environmental, and Architectural Engineering; currently, Fulbright Fellow, Civil Engineering Department, University of Wales, Swansea, Wales, U.K.

Table 1 Strain-gradient coefficients for the lateral displacement polynomial w

i	Term	c_i for w
1	1	w_{rb}
2	x	$\gamma_{yz}/2-q_{rb}$
3	y	$\gamma_{yz}/2+p_{rb}$
4	x^2	$(\gamma_{xz,x}-\epsilon_{x,z})/2$
5	xy	$(-\gamma_{xy,z}+\gamma_{yz,x}+\gamma_{xz,y})/2$
6	y^2	$(\gamma_{yz,y}-\epsilon_{y,z})/2$

Table 2 Strain-gradient coefficients for the in-plane displacement polynomials u and v

i	Term	a_i for u	b_i for v
1	z	$q_{rb}+\gamma_{xz}/2$	$\gamma_{yz}/2-p_{rb}$
2	xz	$\epsilon_{x,z}$	$(\gamma_{xy,z}+\gamma_{yz,x}-\gamma_{xz,y})/2$
3	yz	$(\gamma_{xy,z}-\gamma_{yz,x}+\gamma_{xz,y})/2$	$\epsilon_{y,z}$
4	x^2z	$\epsilon_{x,xz}/2$	$(\gamma_{xy,xz}-\epsilon_{x,yz})/2$
5	xyz	$\epsilon_{x,yz}$	$\epsilon_{y,xz}$
6	y^2z	$(\gamma_{xy,yz}-\epsilon_{y,xz})/2$	$\epsilon_{y,yz}/2$

Each of the eight quantities contained in the strain-gradient coefficient vector $\{\epsilon\}$ produces a specific displacement pattern for the w displacements. For example, in Eq. (1) it can be seen that the displacement field associated with the shear strain γ_{xz} will vary linearly as a function of $x/2$. The strain-gradient coefficients for the complete second-order interpolation polynomials for w, u, and v are given in Tables 1 and 2, respectively. For more information, please see the specified references.

Equation (1) can be generalized to formulate a transformation from nodal degrees of freedom (DOF) to strain-gradient coordinates. This transformation and its inverse are shown as follows:

$$\{d\} = [\phi]\{\epsilon\} \tag{2a}$$

$$\{\epsilon\} = [\phi]^{-1}\{d\} \tag{2b}$$

where $\{d\}$ = the vector of nodal DOF, $\{\epsilon\}$ = the vector of independent strain-gradient coordinates, and $[\phi]$ = the transformation matrix from nodal degrees of freedom to strain-gradient coordinates.

An alternative procedure for formulating finite-element stiffness matrices is available as a result of Eq. (2). The first step in developing this alternate formulation is to transform the strain energy of a finite element in nodal DOF to strain-gradient coordinates

$$\text{S.E.} = \tfrac{1}{2}\{d\}^T[K]\{d\} \tag{3a}$$

$$\text{S.E.} = \tfrac{1}{2}\{\epsilon\}^T[\phi]^T[K][\phi]\{\epsilon\} \tag{3b}$$

$$\text{S.E.} = \tfrac{1}{2}\{\epsilon\}^T[U]\{\epsilon\} \tag{3c}$$

where $[K]$ = the finite-element stiffness matrix and $[U]$ = the coefficient matrix for the strain energy expressed in terms of strain-gradient coordinates. The strain-energy coefficient matrix $[U]$ can be computed directly by substituting the expressions for strain developed from the displacement functions given by Eq. (2) into the following equation for strain energy:

$$\text{S.E.} = \tfrac{1}{2}\int_V (\sigma_x\epsilon_x + \sigma_y\epsilon_y + \sigma_z\epsilon_z + \tau_{xy}\gamma_{xy} + \tau_{xz}\gamma_{xz} + \tau_{yz}\gamma_{yz})\,dV \tag{4}$$

Equation (4) can be integrated and put into matrix notation using the plane stress relations to produce an expresson that has the form of Eq. (3c).

When Eqs. (3b) and (3c) are equated, an alternative procedure for computing finite-element stiffness matrices emerges as

$$[K] = [\phi]^{-T}[U][\phi]^{-1} \tag{5}$$

Equation (5) presents the operational definition for formulating a stiffness matrix in terms of strain-gradient quantities. The stiffness matrix is manipulated in exactly the same way as a standard finite-element stiffness matrix. This formulation procedure is demonstrated later in the text with the formulation of the four-node, 12-DOF rectangular Mindlin plate element.

B. Global and Local Error Measures

The theoretical background required to identify the a priori errors contained in a specific finite element was just presented. Two a priori errors will be identified using this background in a later section.

Procedures for estimating the error in an overall solution, the a posteriori error, will now be discussed. The overall error is estimated by summing the estimated error in the individual elements. This quantitative identification of elements containing high error allows the mesh to be efficiently refined by adding elements to regions of high error. Examples of this procedure and its use to guide mesh refinement are presented in a later section.

The element-by-element error estimates are found as follows. A smoothed set of stress or strain components based on the finite-element solution is computed. The smoothed solution is assumed to be closer to the actual solution than the unmodified finite-element solution because the discontinuities are eliminated. This supposition has been proven for constant strain elements.[6] Proofs for higher-order elements are being attempted.[7]

This procedure for estimating the discretization errors was introduced by Zienkiewicz and Zhu[8] for use in membrane elements. The extension of this method to include plate-bending elements[5] is briefly discussed here.

The error estimate is based on the difference between the approximation to the actual stresses or strains and those found by the finite-element solution. The error estimate, commonly called the "energy norm," is defined for elasticity problems as

$$\|e\| = \left(\int_\Omega (\underline{\sigma}^* - \underline{\sigma}')^T\underline{D}^{-1}(\underline{\sigma}^* - \underline{\sigma}')\,d\Omega\right)^{1/2} \tag{6}$$

where $\|e\|$ = the energy norm, $(\underline{\sigma}^* - \underline{\sigma}')$ = the difference between the smoothed solution and the finite-element solution, and $\underline{D}$ = the constitutive matrix.

The energy norm for individual elements can be written in terms of nodal quantities on the element level as

$$\|e_i\| = \left(\int_{\Omega_e} (\bar{\underline{\sigma}}^{*T}\underline{N}^T\underline{D}^{-1}\underline{N}\,\bar{\underline{\sigma}}^* - \bar{\underline{\sigma}}^{*T}\underline{N}^T\underline{B}\,\bar{\underline{d}} - \bar{\underline{d}}^T\underline{B}^T\underline{N}\,\bar{\underline{\sigma}}^* + \bar{\underline{d}}^T\underline{B}^T\underline{D}\,\underline{B}\,\bar{\underline{d}})\,d\Omega_e\right)^{1/2} \tag{7}$$

where the overbar denotes nodal quantities, $\underline{N}$ the nodal interpolant, $\underline{B}$ the strain-displacement matrix, and $\underline{d}$ the nodal displacement. Equation (7) is used to compute the estimated error in the individual elements. A summation of the errors over the whole problem gives the estimate of the total error. This summation can be interpreted physically as the difference between the absolute value of the energies in the smoothed solutions and the finite-element result.

The form of the error measure given in Eq. (7) can be made more convenient by "normalizing" it with respect to the total

energy contained in the finite-element solution. When this is done, the result is

$$\eta_i = \|e_i\|/\|U\| \times 100 \tag{8}$$

where

$\|e_i\|$ = error energy norm in element i

$\|U\|$ = energy norm for the actual solution over the global domain approximated as

$\|U\| \simeq (\|U'\|^2 + \|e\|^2)^{1/2}$

$\|U'\|$ = energy norm for the finite-element solution over the global domain

The value of η_i for an element gives the percent of the total error contained in the ith element.

The smoothed solution used in this presentation is found in two ways. The first approach determines the smoothed stresses or strains that minimize the square of the difference between the smoothed solution and the finite-element result.[8] This computation is comparable in effort to the computation of the solution of the finite-element problem itself. The second approach smooths the finite-element solution by averaging the stress or strain values at the nodes. This is a very quick computation. The results for these two approaches are compared in a later section and are found to be virtually identical.

III. Formulation of the Mindlin Plate Element

Equation (5) will now be used to derive the stiffness matrix of a four-node, 12-DOF rectangular Mindlin plate element. The element geometry is shown in Fig. 1. The three nodal coordinates at each corner are a transverse displacement w and rotations around the in-plane coordinate axes p and q.

In the standard formulation of the four-node Mindlin element, the independent displacements are given as

$$u = a_1 z + a_2 xz + a_3 yz + a_4 xyz \tag{9a}$$

$$v = b_1 z + b_2 xz + b_3 yz + b_4 xyz \tag{9b}$$

$$w = c_1 + c_2 x + c_3 y + c_4 xy \tag{9c}$$

The linear variation in z contained in u and v incorporates the kinematic constraint that asumes that the cross sections remain planar after deformation. The rotations in a Mindlin plate are defined in terms of the displacements as

$$p = -\frac{\partial v}{\partial z} \tag{10a}$$

$$q = \frac{\partial u}{\partial z} \tag{10b}$$

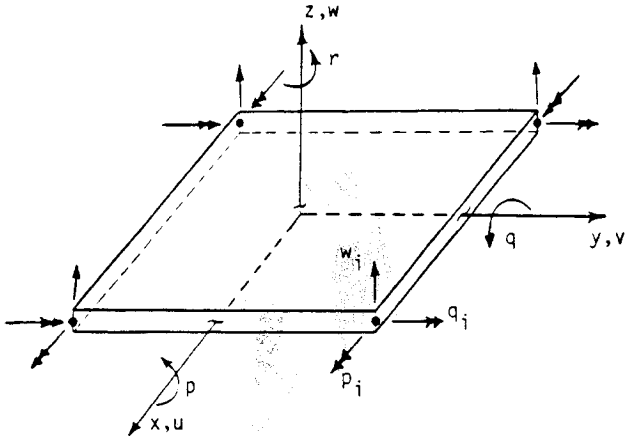

Fig. 1 Geometry for a four-node rectangular Mindlin plane element.

The equivalent interpolation polynomials expressed in strain-gradient notation are given in Tables 1 and 2 as

$$u = (q_{rb} + \gamma_{xz}/2)z + \epsilon_{x,z}xz + (\gamma_{xy,z} - \gamma_{yz,x} + \gamma_{xz,y})/2\,yz + \epsilon_{x,yz}xyz \tag{11a}$$

$$v = (\gamma_{yz}/2 - p_{rb})z + (\gamma_{xy,z} + \gamma_{yz,x} - \gamma_{xz,y})/2\,xz + \epsilon_{y,z}yz + \epsilon_{y,xz}xyz \tag{11b}$$

$$w = w_{rb} + (\gamma_{xz/2} - q_{rb})x + (\gamma_{yz/2} + p_{rb})y + (-\gamma_{xy,z} + \gamma_{yz,x} + \gamma_{xz,y})/2xy \tag{11c}$$

The 12 independent strain-gradient terms contained in Eq. (11) are

$$\{\epsilon\} = [w_{rb} \quad p_{rb} \quad q_{rb}\,\epsilon_{x,z}\,\epsilon_{x,zy}\,\epsilon_{y,z}\,\epsilon_{y,zx}\,\gamma_{xy,z}\,\gamma_{xz}\,\gamma_{xz,y}\,\gamma_{yz}\,\gamma_{yz,x}]^T \tag{12}$$

These 12 quantities are the strain states that this element is capable of modeling. They represent the 12 DOF contained in this element. The use of these strain states as independent variables has the advantage that they have well-defined, physically interpretable meanings.

The expressions for the rotations produced when the displacement functions [Eq. (11)] are substituted into the rotation definitions [Eq. (10)] are

$$p = (p_{rb} - \gamma_{yz}/2) + (\gamma_{xz,y} - \gamma_{xy,z} - \gamma_{yz,x})/2x - \epsilon_{y,z}y - \epsilon_{y,zx}xy \tag{13a}$$

$$q = (q_{rb} + \gamma_{xz}/2) + \epsilon_{x,z}x + (\gamma_{xy,z} - \gamma_{yz,x} + \gamma_{xz,y})/2y + \epsilon_{x,yz}xy \tag{13b}$$

When the displacement functions [Eq. (11)] are substituted into the elasticity definition for small strains, the result is

$$\epsilon_x = \epsilon_{x,z}z + \epsilon_{x,zy}yz \tag{14a}$$

$$\epsilon_y = \epsilon_{y,z}z + \epsilon_{y,xz}xz \tag{14b}$$

$$\gamma_{xy} = \gamma_{xy,z}z + \epsilon_{x,zy}xz + \epsilon_{y,zx}yz \tag{14c}$$

$$\gamma_{xz} = \gamma_{xz} + \epsilon_{x,z}x + \gamma_{xz,y}y + \epsilon_{x,zy}xy \tag{14d}$$

$$\gamma_{yz} = \gamma_{yz} + \gamma_{yz,x}x + \epsilon_{y,z}y + \epsilon_{y,xz}xy \tag{14e}$$

These equations can be written in matrix notation as

$$\{\epsilon'\} = [T]\{\epsilon''\} \tag{15a}$$

where

$$\{\epsilon'\} = [\epsilon_x\,\epsilon_y\,\gamma_{xy}\,\gamma_{xz}\,\gamma_{yz}]^T \tag{15b}$$

$$\{\epsilon''\} = [\epsilon_{x,z}\,\epsilon_{x,zy}\,\epsilon_{y,z}\,\epsilon_{y,zx}\,\gamma_{xy,z}\,\gamma_{xz}\,\gamma_{xz,y}\,\gamma_{yz}\,\gamma_{yz,x}]^T \tag{15c}$$

$$[T] = \begin{vmatrix} z & yz & 0 & 0 & 0 & 0 & 0 & 0 & 0 \\ 0 & 0 & z & xz & 0 & 0 & 0 & 0 & 0 \\ 0 & xz^* & 0 & yz^* & z & 0 & 0 & 0 & 0 \\ x^* & xy^* & 0 & 0 & 0 & 1 & y & 0 & 0 \\ 0 & 0 & y^* & xy^* & 0 & 0 & 0 & 1 & x \end{vmatrix} \tag{15d}$$

The terms marked with the asterisk will be discussed later.

As was seen in Eq. (5), computation of the stiffness matrix requires the formulation of the ϕ and U matrices. The ϕ matrix, which transforms the nodal DOF to strain-gradient coordinates, is developed using Eqs. (11a) and (13). For conve-

nience, the equations used to formulate the ϕ matrix are exhibited in tabular form (see Table 3). This form of the equations clearly shows the displacements and rotations associated with the individual strain states modeled by the Mindlin element. The substitution of the nodal coordinate locations given in Fig. 1 into the functions given in Table 3 results in the ϕ matrix, as defined in Eq. (2a).

The next step in formulating the stiffness matrix is the computation of the strain-energy matrix U. This is accomplished by substituting the expressions for the strains given in Eqs. (14) or (15) into the strain-energy equation [see Eq. (4)]. When this is done, the result has the form of Eq. (3c), where $\{\epsilon\}$ is given by Eq. (12).

With both ϕ and U evaluated, the stiffness matrix can be computed using Eq. (5). The resulting stiffness matrix is identical to the one generated using the standard formulation technique.

Other elements have been developed to demonstrate the versatility of the strain-gradient method.[5] These elements range from Euler-Bernoulli and Timoshenko beam elements to triangular and quadrilateral membrane and plate-bending elements based upon both Kirchhoff and Mindlin plate-bending theories. Application to higher-order elements has also been demonstrated.

IV. Artificial Stiffening in Finite Elements

Two widely documented modeling deficiencies are present in Mindlin plate elements.[3,9-16] These two modeling errors are commonly called parasitic shear and shear locking, respectively.

Parasitic shear is due to the presence of improper terms in the shear strain expression. These improper terms are introduced by the uncritical substitution of the interpolation functions into the strain definitions during the formulation procedure. This error is remedied by eliminating the incorrect terms. These terms are often eliminated in isoparametric elements by evaluating the shear strain energy with a reduced number of integration points. If care is not taken in the use of reduced integration, fictitious zero-energy modes are introduced and desired modeling characteristics are eliminated.[1] If these fictitious zero energy modes are not present, the spurious modeling mechanism called hourglassing cannot exist.

Shear locking is characterized by sharp increases in stiffness and condition number as the relative length (length/thickness) of an element increases. These characteristics are due to a modeling error in the polynomial representation of the shear strains. The interpolation functions introduce constraints that do not exist in the continuum. It has been shown that this modeling deficiency can be controlled in Timoshenko beam elements by introducing a modification based on St. Venant's principle.[3] This modification is currently being added to Mindlin plate elements and will be presented in a later paper.

The source of parasitic shear is identified by inspecting the shear strain expression [Eqs. (14c-14e)]. The γ_{xy} term given by Eq. (14c) will serve as the example. As can be seen, the right-hand side of this equation contains three terms. The first term varies through the thickness and provides the capacity to model a constant moment over the full area of the plate. In addition to varying with z, the next two terms vary with x and y, respectively. If the coefficients of the xz and yz terms were not defined in physical terms, one would be tempted to surmise that these terms represented linear variations of γ_{xy} in the x and y directions. However, it can be seen that these coefficients are normal strain terms. They simply do not belong in a representation of shear strain. In fact, when complete polynomials are utilized in the formulation of an element, as in the case of a triangular element, these normal strain terms are canceled by other coefficients.

Table 3 Displacements and rotation as a function of strain state

	Strain state	w Eq. (11c)	p Eq. (13a)	q Eq. (13b)
1	w_{rb}	1	0	0
2	p_{rb}	y	1	0
3	q_{rb}	$-x$	0	1
4	$\epsilon_{x,z}$	0	0	x
5	$\epsilon_{x,zy}$	0	0	xy
6	$\epsilon_{y,z}$	0	$-y$	0
7	$\epsilon_{y,zx}$	0	$-xy$	0
8	$\gamma_{xy,z}$	$-xy/2$	$-x/2$	$y/2$
9	γ_{xz}	$x/2$	0	1/2
10	$\gamma_{xz,y}$	$xy/2$	$x/2$	$y/2$
11	γ_{yz}	$y/2$	$-1/2$	0
12	$\gamma_{yz,x}$	$xy/2$	$-x/2$	$-y/2$

These erroneous terms are the cause of the artificial stiffening error known as parasitic shear. These terms add strain-energy quantities to the U matrix that make the element overly stiff when it is deformed in flexure. An inspection of Eqs. (14d) and (14e) shows that these expressions also contain parasitic shear terms. The parasitic shear terms are indicated in Eq. (15d) with an asterisk.

When the U matrix for a rectangular element is formed, the following error terms are added due to parasitic shear:

$$u_{44} = E^* a^3 bt/3 \tag{16a}$$

$$u_{55} = E^*(a^3 bt^3 + a^3 b^3 t)/9 \tag{16b}$$

$$u_{66} = E^* ab^3 t/3 \tag{16c}$$

$$u_{77} = E^*(ab^3 t^3 + a^3 b^3 t)/9 \tag{16d}$$

where

$$E^* = E/2(1+\nu)$$

The subscripts in the preceding strain-energy terms refer to the normal strains in the order given in Eq. (12).

The characteristics of the errors produced by parasitic shear will be illustrated with the example of the modeling defect produced in the $\epsilon_{x,z}$ deformation mode by parasitic shear. The error is computed by dividing the error term given in Eq. (16a) by the correct term, $(E/(1-\nu^2))abt^3/3$. When this is done, the final result is

$$\text{Error Ratio} = ((1-\nu)/2)(a/t)^2 \tag{17}$$

It can be seen that this error is strongly dependent on the element dimensions and should be removed to insure accurate results. It is apparent that, for thin sections, the error is quite significant.

The use of strain-gradient notation allows the parasitic shear terms to be removed before the strain-energy expression is computed. This is done by simply removing the incorrect terms from the expression for strain energy and proceeding with the formulation procedure.

This direct approach is not possible in the isoparametric formulation procedure. The erroneous terms are buried in the undefined coefficients. However, the parasitic shear terms can be eliminated by the judicious application of a reduced number of integration points in the numerical integration scheme used to evaluate the strain-energy expressions. In the case of the shear strain γ_{xy} given in Eq. (14c), the two parasitic shear terms can be removed by using reduced integration for the integration in the x and y directions. However, if reduced integration is used in the x and y direction in Eqs. (14d) and (14e), terms desired in the analysis will be removed. In Eq. (14d), the term $\gamma_{xz,y}$ would be eliminated. In Eq. (14e), the term $\gamma_{yz,x}$ would be eliminated. If these terms are eliminated, the resulting stiffness matrix exhibits two spurious rigid-body modes.[12] In order to eliminate only the parasitic shear terms in Eq. (14d), reduced integration should only be used in the x direction. Similarly, the parasitic shear terms are removed from Eq. (14e) if reduced

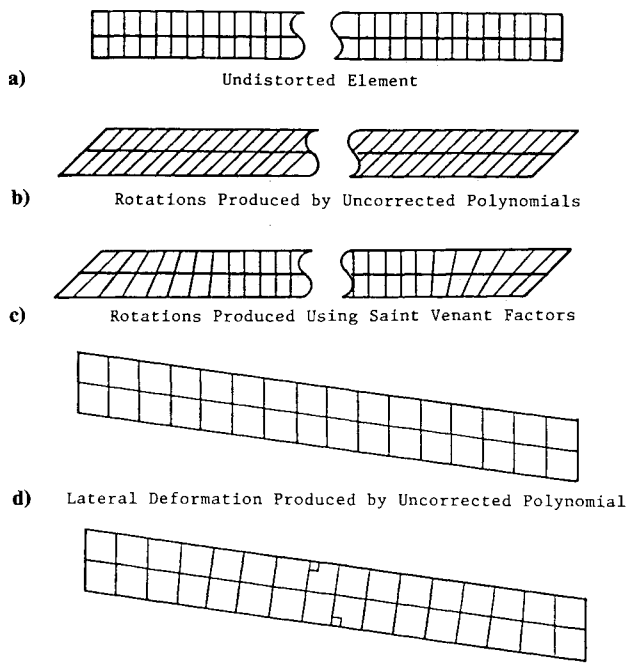

Fig. 2 Possible modes of shear modeling in long elements.

integration is used in the y direction. Thus, it can be seen that the blind application of reduced integration to this element would eliminate desirable terms and introduce new modeling deficiencies.

Selectively reduced integration has been used[13] to avoid the inclusion of zero-energy modes in plate-bending elements. However, this method of using strain-gradient notation has illustrated why the method of selectively reduced integration does not introduce spurious rigid-body modes into the stiffness matrix of the element.

Shear locking is caused by a modeling error in the out-of-plane shear strains that increases with the relative length. This phenomenon occurs even if parasitic shear has been eliminated and can be easily demonstrated with the example of the stiffness matrix of a cantilevered Timoshenko beam:

$$[K]_{\text{Total}} = [K]_{\text{Flexure}} + [K]_{\text{Shear}} \tag{18a}$$

where

$$[K]_{\text{Flexure}} = EI \begin{vmatrix} 0 & 0 \\ 0 & 1/L \end{vmatrix} \tag{18b}$$

$$[K]_{\text{Shear}} = KG \begin{vmatrix} 1/L & -1/2 \\ -1/2 & L/4 \end{vmatrix} \tag{18c}$$

The parasitic shear terms have been removed from this element.

As can be seen, the flexure component of the stiffness matrix decreases as the length increases. In the shear component, one diagonal quadrant decreases while the other increases with the increase in length. The effect of this is to stiffen the overall result. This stiffening is counter to the expected result. In physical systems, the shear effect is reduced as the length of the beam increases.

By backtracking through the derivation of the stiffness matrix, the term that causes the shear locking characteristics is found to be due to the $\partial u/\partial y$ component of the shear strain.[3] The following physical considerations account for this increase.

Figure 2a shows a long, thin, undistorted beam. When the ends of the element are given a rotation that in this model is equal to $-\partial u/\partial y$, the shear deformation continues unattenuated, as shown in Fig. 2b. This is a result of a constraint imposed by the interpolation function used to represent the continuum.

In actual physical systems, this type of behavior does not occur. The behavior of a physical beam would be more like the situation depicted in Fig. 2c. The rotations would diminish as they moved into the element. The strain energy and stiffness of the system would not increase linearly with the length beyond a certain point.

This artificial stiffening imposed by the interpolation model can be removed by introducing a factor into the $\partial u/\partial y$ term of the shear strain based on St. Venant's principle. However, equilibrium considerations require that the same factor be applied to the $\partial v/\partial x$ term in the shear strain definition. This correction would affect the upper left-hand quadrant of Eq. (18c). The question is whether this correction would be consistent with the actual physical system.

Without the St. Venant correction factor, the deformation of the beam element is as shown in Fig. 2d. Every portion of the element undergoes distortion. The stiffness, however, does not increase with length because the amount of distortion decreases as the element gets longer. When the St. Venant factor is included, the deformation is as shown in Fig. 2e. Only the portions of the beam near the ends are distorted. This would correspond to the physical concept embodied in St. Venant's principle. Thus, it can be concluded that the incorporation of a factor based on St. Venant's principle would not introduce a new source of error into the finite-element model.

Now that the cause of shear locking has been introduced and a correction for the modeling error has been presented, it remains to show that the same concepts apply to the Mindlin plate element.

The stiffness matrix for the four-node Mindlin element developed in Sec. III has been formulated in symbolic form using the symbol manipulation program MACSYMA. In order to reduce the size of the matrices that must be shown, the elements of a cantilevered plate will be used in this discussion. Nodes 1 and 4 of the element shown in Fig. 1 will be fixed. The element will be given a unit width in the y direction. The length in the x direction, a, will be retained as a parameter. The conclusions reached for the cantilevered plate are applicable to an unrestrained element.

The shear stiffness contribution to the overall stiffness matrix will be presented first. This corresponds to Eq. (18c) for the beam element and is given as

$$[K]_{\gamma_{xz}} = E^* \begin{vmatrix} \frac{1}{4a}+\frac{1}{12a} & & & & & \\ \frac{1}{4a}-\frac{1}{12a} & \frac{1}{4a}+\frac{1}{12a} & & & \text{SYM} & \\ 0+0 & 0+0 & 0+0 & & & \\ 0+0 & 0+0 & 0+0 & 0+0 & & \\ \frac{1}{8}+\frac{1}{24} & \frac{1}{8}-\frac{1}{24} & 0+0 & 0+0 & \frac{a}{16}+\frac{a}{48} & \\ \frac{1}{8}-\frac{1}{24} & \frac{1}{8}+\frac{1}{24} & 0+0 & 0+0 & \frac{a}{16}-\frac{a}{48} & \frac{a}{16}+\frac{a}{48} \end{vmatrix} \tag{19}$$

The first term in each matrix element is due to the γ_{xz} strain state and the second is due to $\gamma_{xz,y}$. Both of these contributions have the same form as the shear contribution of the beam. As a result, the overall stiffness increases as the parameter a gets larger. This also means that the artificial stiffening introduced by these strain states can be corrected by applying a St. Venant factor to this stiffness contribution.

The stiffness contribution of the flexure strain states $\epsilon_{x,z}$ and $\epsilon_{x,zy}$ are the following:

$$[K]_{\epsilon_x} = E_1 \begin{vmatrix} 0+0 & & & & & & \\ 0+0 & 0+0 & & & & & \\ 0+0 & 0+0 & 0+0 & & \text{SYM} & & \\ 0+0 & 0+0 & 0+0 & 0+0 & & & \\ 0+0 & 0+0 & 0+0 & 0+0 & \frac{1}{4a}+\frac{a}{12} & & \\ 0+0 & 0+0 & 0+0 & 0+0 & \frac{1}{4a}-\frac{a}{12} & \frac{1}{4a}+\frac{a}{12} & \end{vmatrix} \tag{20}$$

Where $E_1 = E/(1-\nu^2)$. The first term in each element is due to the $\epsilon_{x,z}$ strain state. This component decreases as the dimension a increases so that no correction is required. The second term in each element is due to $\epsilon_{x,zy}$.

As can be seen, this second element grows as the dimension a increases. The effect of this is to stiffen the overall result in the same manner as the $L/4$ term in the beam element [see Eq. (18c)]. When the deformation pattern of this strain state is studied, it is found to have the same character as the shear component discussed in Figs. 2a–2c. Thus, it can be corrected with a St. Venant factor. A similar correction can be introduced in the x direction and will be presented in a later paper.

Other approaches have been used to control the unwanted characteristics of shear locking by controlling the growth of the shear locking effects. MacNeal[14] uses a "residual bending flexibility" to control the shear locking effects. Pugh et al.[15] proposed an artificial plate thickness for very thin plates that avoids any numerical instability problems that may occur due to shear locking. Tessler and Hughes[16] use a deflection matching scheme to develop a modified shear correction factor to control the shear strain energy.

V. Error Analysis Applied to Plate Problems

Procedures for estimating the errors occurring in the results for finite-element analyses of plate problems are demonstrated in this section. As discussed earlier, the error occurring in each element can be estimated as the difference between the energy norms of the discontinuous finite-element solution and an improved superconvergent solution. The improved solution can be generated by many techniques.[17-20] Two methods used here are a global smoothing routine[8] that forms a continuous stress solution over the entire global domain and a local nodal stress-averaging method. The global method involves a solution of a system of equations that may become prohibitive in terms of cost for large problems. However, the nodal stress-averaging scheme is a quick and efficient method that produces a continuous stress solution using the stress results of each element.

With an improved solution for each element, the elemental errors can be computed using Eq. (7). The global estimate of the error can be summed for all the elements as

$$\|e\| = \left(\sum_{i=1}^{\text{ELEM}} e_i^2 \right)^{1/2} \tag{21}$$

The elemental error measures are used to identify regions of high error. This information is used to improve the modeling to produce results with an improved overall error measure.

The effectiveness of the error-estimating procedure is illustrated with an example plate problem modeled using Mindlin plate-bending elements. Both four-node quadrilaterals and 12-DOF triangular elements are used in the models. The problem used to illustrate the error-estimating procedure is the familiar square-plate problem with a concentrated centerload and simply supported edges. Due to symmetry, only a quarter of the plate is used in the analysis, and the mesh descriptions in the tables presenting the results refer to this quarter-section.

The problem is analyzed using both the strian gradient and standard isoparametric elements. For the strain-gradient elements, both the element with and without parasitic shear is used. For the isoparametric elements, both full and reduced integration is utilized. The reduced integration is applied to all the shear strains and results in an element that has two additional zero-energy modes of deformation. The reduced integration erroneously removed two strain states from the basis description of the element. It is the removal of these two strain states that produces the two extra zero-energy modes. With rectangular elements, the isoparametric element with full integration and the strain-gradient element with parasitic shear will give identical results.

The transverse deflections under the point load for analyses using the various elements are given in Table 4. The immense improvement in the results produced by eliminating the parasitic shear term is evident from the results in the table. The parasitic shear terms severely stiffen the elements that contain this modeling deficiency.

The estimates of the global error using both local and global smoothing procedures are presented in Table 5 for this plate problem performed with the underintegrated isoparametric Mindlin quadrilateral element. Elements with the parasitic shear terms removed are used since these erroneous terms stiffen the element so drastically that the results are always so poor, as illustrated in the deflections given in Table 3. The underintegrated isoparametric Mindlin element is used here since it is found in many commercially available codes.

It is noted that if these elements are used in commercial codes, then they are used in conjunction with some form of "hourglass control" to stabilize the spurious modes. Also, the exact error in Table 5 is the error in the energy norm of the

Table 4 Results of square-plate analyses using four-node Mindlin plate elements

Mesh in quadrant	Deflections under point load		
	Element 1[a]	Element 2[b]	Element 3[c]
1×1	4.278E-5	1.341E-2	2.405E-2
2×2	1.343E-4	1.167E-2	1.262E-2
4×4	4.846E-4	1.160E-2	1.181E-2
8×8	1.690E-3	1.162E-2	1.170E-2
12×12	3.203E-3	1.163E-2	1.170E-2
Exact deflection[d]		1.160E-2	

[a]Element 1: strain gradient element with all terms (also isoparametric element with 2 × 2 Gauss numerical integration).
[b]Element 2: strain gradient element without the parasitic shear terms.
[c]Element 3: isoparametric Mindlin element with reduced integration (1 × 1) for all shear expressions.
[d]Exac: solution for thin-plate theory.

Table 5 Discretization error estimates of energy norms for square-plate analyses using four-node Mindlin Plate Elements

Mesh in quadrant	Exact error %	Estimated percentage error: Global smoothing	Estimated percentage error: Local nodal averaging
2×2	29.6	20.6	24.0
4×4	13.3	17.4	19.2
8×8	9.4	12.0	12.8
12×12	9.3	9.95	10.5

finite-element solution as compared with the energy norm of the thin-plate solution.

The global errors predicted by the error analysis are seen to give accurate estimates of the exact error as the solution approaches the true solution. The poor estimates for the first discretization are due to the coarseness of the mesh, which has only one interior nodal point with which to smooth the stress solution.

It is noted that the error in energy norm is larger than the error given in terms of strain energy. The error in strain energy can be shown to be the square of the error in energy norm, which means that an error of 10% in energy norm corresponds to a 1% error in strain energy. This is verified by Table 3, where due to the single load on the plate, the deflection under the point load is indicative of the strain energy in the solution. As the discretization is refined, the error in the deflections is less than 1%.

The estimated error using the global smoothing technique is always slightly less than that for the local nodal averaging scheme. This is a direct result of the global method being a least-squares minimization of the difference between the finite element and improved solutions.

This problem is also analyzed using a 12-DOF triangular Mindlin plate element. The 12 DOF consist of six transverse displacements at the corner and midside nodes and two rotations at each of the three corner nodes. The element is derived using strain-gradient notation using the following displacement interpolation functions:

$$w(x,y) = [w] + [\gamma_{xz}/2 - q]x + [\gamma_{yz}/2 + p]y + [\gamma_{xz,x} - \epsilon_{x,z})/2]x^2 + [(-\gamma_{xy,z} + \gamma_{yz,x} + \gamma_{xz,y})/2]xy + [(\gamma_{yz,y} - \epsilon_{y,z})/2]y^2 \quad (22)$$

$$u(x,y,z) = [\gamma_{xz}/2 + q]z + [\epsilon_{x,z}]xz + [(\gamma_{xy,z} - \gamma_{yz,x} + \gamma_{xz,y})/2]yz \quad (23)$$

$$v(x,y,z) = [\gamma_{yz}/2 - p]z + [(\gamma_{xy,z} + \gamma_{yz,x} - \gamma_{xz,y})/2]xz + [\epsilon_{y,z}]yz \quad (24)$$

Application of strain-displacement definitions yield the following strain expressions:

$$\epsilon_x = [\epsilon_{x,z}]z \quad (25)$$

$$\epsilon_y = [\epsilon_{y,z}]z \quad (26)$$

$$\gamma_{xy} = [\gamma_{xy,z}]z \quad (27)$$

$$\gamma_{xz} = [\gamma_{xz}] + [\gamma_{xz,x}]x + [\gamma_{xz,y}]y \quad (28)$$

$$\gamma_{yz} = [\gamma_{yz}] + [\gamma_{yz,x}]x + [\gamma_{yz,y}]y \quad (29)$$

This element has no parasitic shear terms associated with it, as is evident from the shear strain expressions given in Eqs. (27-29). Furthermore, its geometry, being triangular in shape, eliminates any difficulties associated with interelement compatibility during the mesh refinement process. This avoids the use of kinematic constraints usually required for an adaptive refinement process using quadrilateral elements. However, the use of these triangular elements is expected to give slow convergence due to the nature of the strain distributions as given in Eqs. (25-29). It is seen that the in-plane strains resemble those for the constant strain triangular (CST) membrane element, which is usually avoided due to slow convergence.

For the triangular element, an adaptive process is utilized whereby the elemental error estimates for the previous discretization are used in guiding the refinement for the next discretization. The elemental errors are normalized by Eq. (8), and these quantities are used to guide the mesh refinement. If the elemental error is over a certain user-specified percentage of the maximum elemental error, then the element is a candidate for subdivision. The subdivision algorithm consists of subdividing an element into two elements with the subdivision occurring along the longest side in the triangular element. If the longest side of the element to be divided is not on the boundary, then the adjacent element is also divided in order to maintain compatibility. More efficient refinement strategies

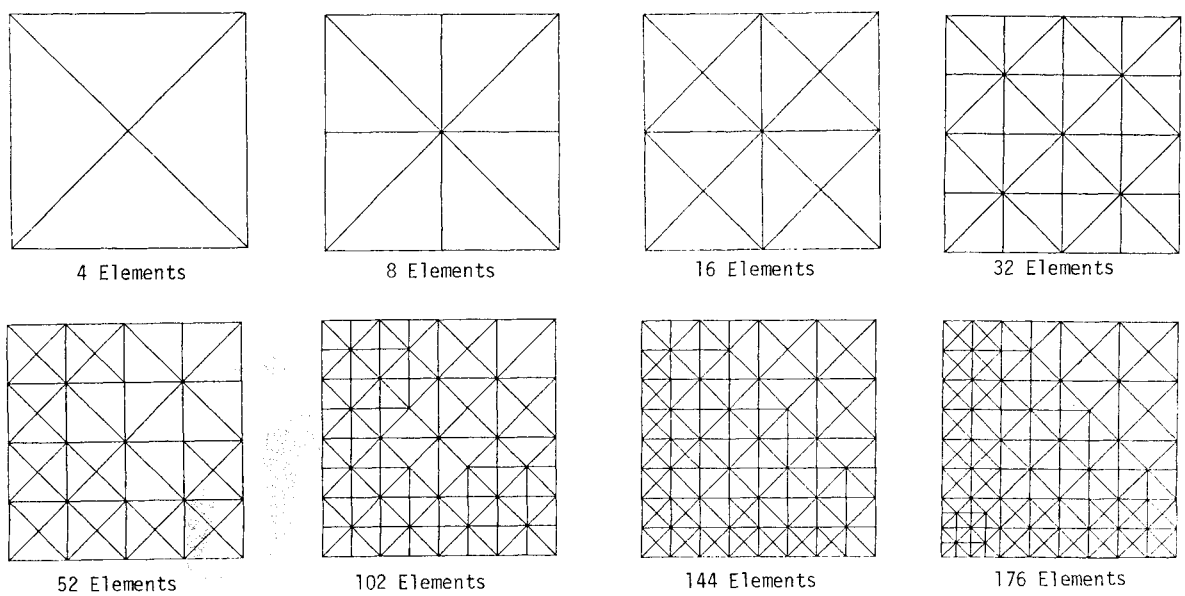

Fig. 3 Simply supported square plate with centerload, initial, and automatically refined meshes (upper right quadrant shown, load at bottom left).

Table 6 Results of adaptive refinement process on simply supported square plate with a concentrated load using triangular Mindlin elements

Elements in quarter-mesh	Center deflection	Percentage error in energy norms	
		Exact	Estimated
4	0.783E-2	57.0	44.6
8	0.786E-2	56.8	37.6
16	0.01010	35.4	27.9
32	0.01052	30.5	24.1
52	0.01106	21.6	18.2
102	0.01131	15.7	14.0
144	0.01144	11.7	11.5
176	0.01151	9.0	9.9

are available. For example, methods for reaching a desired level of accuracy in one mesh refinement for membrane problems are available[8] and could be extended to plate problems. However, the objective of this research is to validate the fact that mesh refinement guided by this error-estimating procedure produces convergent results.

The initial model is only required to sufficiently represent the continuum with loads and boundary conditions. The elemental errors guide the automated refinement process, which stops when the estimated global error is within a user-specified accuracy criterion. For this triangular element, the nodal averaging scheme is used.

The initial mesh of the upper right quadrant for the previous problem and the subsequent idealizations produced by the adaptive refinement process are shown in Fig. 3. In this adaptive process an element is subdivided when the error is over 20% of the maximum elemental error. The deflections under the load and the exact and estimated global errors in energy norms are given in Table 6. The convergence of the center deflection, indicative of the strain energy, to the exact deflection is evident from the table with the error in the deflection (strain energy) being less than 1.0% in the final idealization.

The effectiveness of the error estimation procedure is illustrated in the table with the difference in the actual and the estimated errors in energy norms being reduced as the solution converges to the exact solution. The adaptive refinement procedure would continue until the global error estimate reduced to within a user-specified accuracy tolerance, specified in either strain energy or energy norm error.

This illustrates the procedure envisioned for the use of adaptive refinement. A coarse discretization that sufficiently defines the continuum is generated, and then the subsequent idealizations are automatically generated using the a postpriori error analysis. The elemental error indicators are used to guide the refinement in areas of high error and the global error estimate used to define the accuracy in the current idealization. The process is repeated until an adequate user-specified accuracy is obtained. With this type of procedure, even inexperienced analysts may realize greater confidence in the approximations given by the finite-element method.

VI. Summary and Conclusion

This paper has presented procedures for eliminating errors in finite-element analysis of plate problems by removing modeling deficiencies in individual elements (a priori error analysis) and by identifying regions of high error in the computed results (a posteriori error analysis). The a priori error analysis identifies errors in the individual finite elements during the formulation process through the use of physically based strain-gradient notation. The use of this notation also provides guidance in eliminating these elemental modeling deficiencies from the elements.

Specifically, the sources of parasitic shear, hourglassing, and shear locking have been identified. Rationale for definitively eliminating parasitic shear and hourglassing have been presented. It seems very likely that the shear correction factors introduced by Tessler and Hughes[16] to reduce the shear strain energy can be explained in terms of the St. Venant factor discussed here and in Ref. 3. If so, a physically based criterion for controlling shear locking is currently available.

The use of these physically based criteria for eliminating inherent modeling deficiencies eliminates the need to modify elements based on the solution of a few specific problems. The elimination of this approach, commonly called "cooking" elements, will put the element formulation process on a more rational basis. This will make the results more widely useable.

The error-estimating procedure presented here provides a method for validating and improving finite-element solutions. The adaptive refinement algorithm applied here is quite crude. Its purpose was to demonstrate that improved solutions would be produced when mesh refinement was guided by the error analysis procedures presented here. Other approaches to mesh refinement that produce a desired level of accuracy after one mesh refinement have been demonstrated for membrane problems.[8] Similar refinement strategies are being developed by the authors of this paper for plate problems.

The elements and error analysis procedures developed here are easily added to existing codes. The use of such procedures to identify errors in finite-element solutions will allow the analysis step to be incorporated in automated design applications with confidence. This will assist computer-aided design to come closer to its goal of reducing the level of specialized expertise required by the designer.

Acknowledgments

The authors gratefully thank the Civil Engineering Department at the University College of Swansea, University of Wales for the use of their facilities and for their hospitality during the academic year 1986/87. The junior author would like to express his appreciation to the Fulbright Commission for making his stay in Swansea possible. Both authors would like to acknowledge the current support provided by a grant from the Computational Structural Mechanics Program (NAG-1-802) administered at the NASA Langley Research Center.

References

[1]Dow, J. O. and Byrd, E. E., "An Exact Energy Plate Finite Element," *Proceedings of the 27th AIAA/ASME/ASCE/AHS Structures, Structural Dynamics, and Materials Conference,* AIAA, New York, 1986, pp. 1–7.

[2]Dow, J. O., Cabiness, H. D., and Ho, T. H., "A Linear Strain Element with Curved Edges," *ASCE Journal of Structural Engineering,* Vol. 112, No. ST4, April 1986, pp. 692–708.

[3]Dow, J. O. and Byrd, D. E., "The Identification and Elimination of Artificial Stiffening Errors in Finite Elements," *International Journal for Numerical Methods in Engineering,* Vol. 26, March 1988, pp. 743–762.

[4]Dow, J. O., Cabiness, H. D., and Byrd, E. E., "An Exact Energy Finite Element," Paper 85-0766-CP, AIAA/ASME/ASCE/AHS 26th Structures, Structural Dynamics, and Materials Conference, AIAA, New York, 1985.

[5]Byrd, D. E., "Identification and Elimination of Errors in Finite Element Analysis," Ph.D. Dissertation, University of Colorado, Boulder, CO, 1988.

[6]Wheeler, M. F. and Whiteman, J. R., "Superconvergent Recovery of Gradients on Subdomains from Piecewise Linear Finite Element Approximations," *Numerical Methods for Partial Differential Equations,* Vol. 3, Jan. 1987, pp. 65–82.

[7]Whiteman, J. R., Personal communication, 1986.

[8]Zienkiewicz, O. C. and Zhu, J. Z., "A Simple Error Estimator and Adaptive Procedure for Practical Engineering Analysis," *International Journal for Numerical Methods in Engineering,* Vol. 24, Feb. 1987, pp. 337–357.

[9]Zienkiewicz, O. C., Taylor, R. L., and Too, J. M., "Reduced Integration Techniques in General Analysis of Plates and Shells," *International Journal for Numerical Methods in Engineering,* Vol. 3, No. 2, April–June 1971, pp. 275–290.

[10]Zienkiewicz, O. C., *The Finite Element Method,* 3rd ed., Sec. 11.6, McGraw-Hill, London, 1977.

[11]Huang, H. C. and Hinton, E., "A Nine Node Lagrangian Mindlin Plate Element with Enhanced Shear Interpolation," *Engineering Computation,* Vol. 1, Dec. 1984, pp. 369-379.

[12]Cook, R. D., *Concepts and Applications of Finite Element Analysis,* 2nd ed., Wiley, New York, 1981, pp. 263-266.

[13]Pawsey, S. F. and Clough, R. W., "Improved Numerical Integration of Thick Shell Finite Elements," *International Journal for Numerical Methods in Engineering,* Vol. 3, No. 4, Oct. 1971, pp. 575-586.

[14]MacNeal, R. H., "A Simple Quadrilateral Shell Element," *Computers and Structures,* Vol. 8, April 1978, pp. 175-183.

[15]Pugh, E. D. L., Hinton, E., and Zienkiewicz, O. C., "A Study of Quadrilateral Plate Bending Elements With 'Reduced' Integration," *International Journal for Numerical Methods in Engineering,* Vol. 12, July 1978, pp. 1059-1079.

[16]Tessler, A. and Hughes, T. J. R., "An Improved Treatment of Transverse Shear in the Mindlin-Type Four-Node Quadrilateral Element," *Computer Methods in Applied Mechanics and Engineering,* Vol. 39, No. 3, Sept. 1983, pp. 311-335.

[17]Hinton, E. and Campbell, J. S., "Local and Global Smoothing of Discontinuous Finite Element Functions Using a Least Square Method," *International Journal for Numerical Methods in Engineering,* Vol. 8, No. 3, 1974, pp. 461-480.

[18]Zlamal, M., "Superconvergence and Reduced Integration in the Finite Element Method," *Mathematics of Computation,* Vol. 32, July 1978, pp. 663-685.

[19]Loubignac, G., Cantin, G., and Touzot, G., "Continuous Stress Fields in Finite Element Analysis," *AIAA Journal,* Vol. 15, Nov. 1977, pp. 1645-1647.

[20]Zienkiewicz, O. C., Li, X., and Nakazawa, S., "Iterative Solution of Mixed Problems and the Stress Recovery Procedures," *Communications in Applied Numerical Methods,* Vol. 1, Jan. 1985, pp. 3-9.